

Electronic structures and topological properties in nickelates $Ln_{n+1}Ni_nO_{2n+2}$

Jiacheng Gao,^{1,2} Shiyu Peng,^{1,2} Zhijun Wang,^{1,2,*} Chen Fang,^{1,2,†} and Hongming Weng^{1,2,3,4,5,‡}

¹*Beijing National Laboratory for Condensed Matter Physics,*

Institute of Physics, Chinese Academy of Sciences, Beijing 100190, China

²*School of Physical Sciences, University of Chinese Academy of Sciences, Beijing 100190, China*

³*Songshan Lake Materials Laboratory, Dongguan, Guangdong 523808, China*

⁴*CAS Centre for Excellence in Topological Quantum Computation, Beijing, China*

⁵*Physical Science Laboratory, Huairou National Comprehensive Science Center, Beijing, China*

After the significant discovery of the hole-doped nickelate compound $Nd_{0.8}Sr_{0.2}NiO_2$, an analysis of the electronic structure, orbital components, Fermi surfaces and band topology could be helpful to understand the mechanism of its superconductivity. Based on the first-principles calculations, we find that Ni $3d_{x^2-y^2}$ states contribute the largest Fermi surface. Ln $5d_{3z^2-r^2}$ states form an electron pocket at Γ , while $5d_{xy}$ states form a relatively bigger electron pocket at A. These Fermi surfaces and symmetry characteristics can be reproduced by our two-band model, which consists of two elementary band representations: $B_{1g}@1a \oplus A_{1g}@1b$. We find that there is a band inversion near A, giving rise to a pair of Dirac points along A–M below the Fermi level once including spin-orbit coupling. Furthermore, we have performed the LDA+Gutzwiller calculations to treat the strong correlation effect of Ni 3d orbitals. In particular, the bandwidth of $3d_{x^2-y^2}$ has been renormalized largely. After the renormalization of the correlated bands, the Ni $3d_{xy}$ states and the Dirac points become very close to the Fermi level. Thus, a hole pocket at A could be introduced by hole doping, which may be related to the observed sign change of Hall coefficient. By introducing an additional Ni $3d_{xy}$ orbital, the hole-pocket band and the band inversion can be captured in our modified model. Besides, the nontrivial band topology in the ferromagnetic two-layer compound $La_3Ni_2O_6$ is discussed and the band inversion is associated with Ni $3d_{x^2-y^2}$ and La $5d_{xy}$ orbitals.

INTRODUCTION

After the discovery of high- T_c superconductivity in the cuprates[1, 2], mixed-valent nickelates with similar crystal and electronic configurations as cuprates have been attracting lots of attention [3]. In particular, the configuration of Ni^{+} in infinite-layer nickelates $LnNiO_2$ ($Ln=La, Nd, Pr$) is almost identical to that of Cu^{++} in the parent compounds of cuprates. Although much effort has been devoted along this direction in the past two decades, it remains elusive for the possible superconductivity in mixed-valent nickelates. Until very recently, the superconductivity with $T_c = 9 \sim 15K$ was discovered in hole-doped $Nd_{0.8}Sr_{0.2}NiO_2$ for the first time[4]. For the parent compound $NdNiO_2$, previous studies have established several experimental facts that are distinct from the parent compound of cuprates. First, no long-range magnetic order is observed experimentally[5, 6], while an antiferromagnetically ordered state is formed in the cuprates[7]. Second, $NdNiO_2$ exhibits a metallic behavior above 50K[4], while the parent cuprates are Mott insulators[8]. Third, the superconductivity (so far) is only found in the hole-doped $Nd_{0.8}Sr_{0.2}NiO_2$, while it is found in the electron-doped cuprate $Sr_{1-x}La_xCuO_2$ in the same structure[9]. These experimental facts indicate that the ground state of the parent nickelates could have significant difference from the cuprates. The analysis of their electronic band structures, orbital components, Fermi surfaces, and the band topology are wanted. In addition, a minimal-band effective model is very helpful to further understand the mechanism of superconductivity.

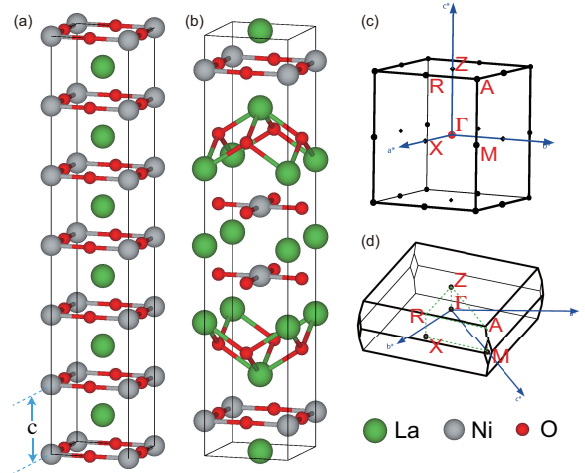


FIG. 1: (Color online) Crystal structures and Brillouin zones. The crystals of infinite-layer compound $LaNiO_2$ ($P4/mmm$) and two-layer compound $La_3Ni_2O_6$ ($I4/mmm$) are presented in (a) and (b), respectively. (a) contains six unit cells (c is the lattice parameter in z direction). The primitive reciprocal lattice vectors and high-symmetry k -points are indicated in the first Brillouin zones of $LaNiO_2$ (c) and $La_3Ni_2O_6$ (d).

In this work, we have performed detailed first-principles calculations within the framework of density functional theory (DFT/LDA). The obtained band structure of the parent(un-doped) compound $NdNiO_2$ is similar to that of $LaNiO_2$ reported previously [10] and $PrNiO_2$ ($Nd-4f$ and $Pr-4f$ orbitals are treated as core states.). In this article, $LaNiO_2$ is taken as a representa-

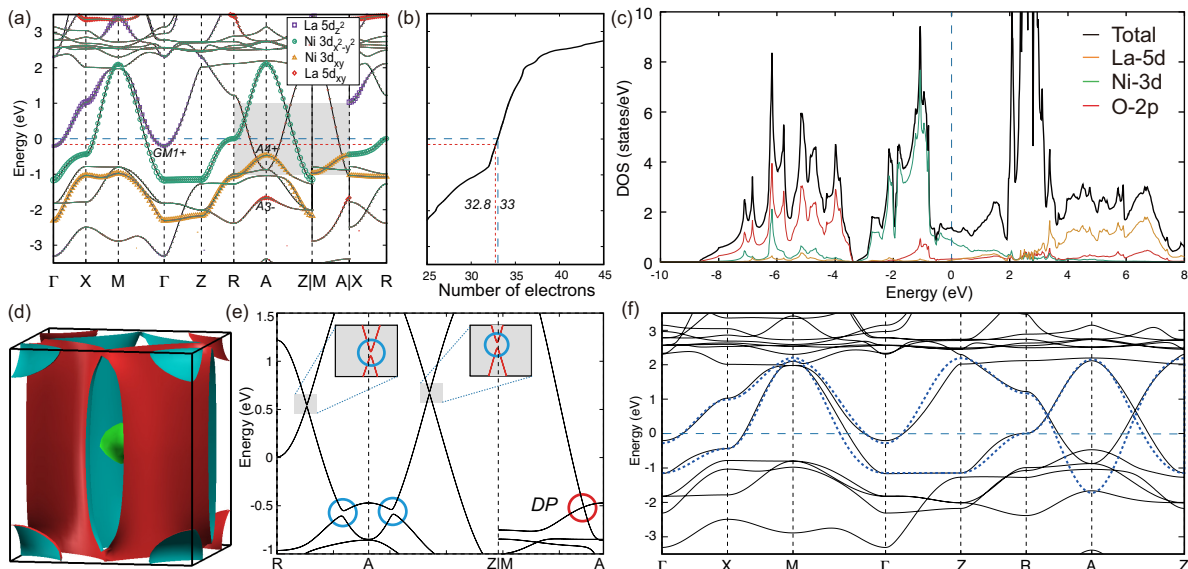


FIG. 2: (Color online) (a) The band structure of LaNiO_2 without SOC. The weights of $\text{La } 5d_{z^2}$, $\text{Ni } 3d_{x^2-y^2}$, $\text{Ni } 3d_{xy}$ and $\text{La } 5d_{xy}$ states are indicated by the size of the purple squares, green circles, yellow triangles and red diamonds, respectively. The $\text{La } 5d_{z^2}$ band at Γ is labeled by $GM1+$, while the $\text{Ni } 3d_{xy}$ and $\text{La } 5d_{xy}$ bands at A are labeled by $A4+$ and $A3-$, respectively. The blue dashed line represents the Fermi level E_F and the red dashed line represents the estimated chemical potential in the hole doped $\text{Nd}_{0.8}\text{Sr}_{0.2}\text{NiO}_2$. The total number of electrons as a function of chemical potential is plotted in (b). The partial density of states (DOS) is given in (c). The Fermi surfaces of LaNiO_2 are shown in (d). In the band structure with SOC (e), the crossings in the shadowed area of (a) are gapped except the Dirac point (DP) along $M-A$. The bands of our two-band model are shown as blue dashed lines in (d).

tive and the band structures of NdNiO_2 and PrNiO_2 are presented in the Supplemental Material (SM). In the undoped case, there are three bands intersecting the Fermi level (E_F), mainly from $\text{Ni } 3d_{x^2-y^2}$, $\text{La } 5d_{xy}$ and $\text{La } 5d_{3z^2-r^2}$ orbitals. They form a large cylinder-like electron pocket (EP) surrounding the Γ - Z line, a sphere-like EP at A , and a comparatively smaller sphere-like EP at Γ , respectively. These Fermi surfaces and symmetries can be reproduced by our two-band model, which consists of two elementary band representations (EBRs): $B_{1g}@1a \oplus A_{1g}@1b$. The EBR of $B_{1g}@1a$ refers to $3d_{x^2-y^2}$ orbital at Wyckoff site $1a$, while the EBR of $A_{1g}@1b$ refers to A_{1g} orbital at Wyckoff site $1b$, where no atoms sit.

We find a band inversion near A happens between the $\text{Ni } 3d_{xy}$ states and $\text{La } 5d_{xy}$ states (The effect of Coulomb interaction U is discussed in the SM). With small U and spin-orbital coupling (SOC), it gives rise to a pair of Dirac points along $A-M$. After considering the renormalization of $\text{Ni } 3d$ bands, the Dirac point becomes very close to the charge neutrality level (E_F) and accessible by hole doping. As a result, a hole pocket (HP) may emerge at A , which may be responsible for the sign change of Hall coefficient in the experiment [4]. By introducing an additional $\text{Ni } 3d_{xy}$ orbital, the hole-pocket band and the band inversion can be captured in the modified model. Besides, the nontrivial band topology in the ferromagnetic two-layer ($n = 2$) compound $\text{La}_3\text{Ni}_2\text{O}_6$ is discussed

and a band inversion happens between $\text{Ni } 3d_{x^2-y^2}$ and $\text{La } 5d_{xy}$ orbitals.

CRYSTAL STRUCTURE AND METHODOLOGY

The parent compound LaNiO_2 can be obtained from the perovskites LaNiO_3 by removing the apical oxygens, as shown in Fig. 1(a). Consequently, it has a tetragonal lattice, and has the same planes as the cuprate superconductors with Ni^{2+} instead of Cu^{2+} ions. Similarly, the two-layer nickelate $\text{La}_3\text{Ni}_2\text{O}_6$ [in Fig. 1(b)] can be produced [11] from the two-layer perovskite $\text{La}_3\text{Ni}_2\text{O}_7$. We performed the first-principles calculations with VASP package [12, 13] based on the density functional theory with the projector augmented wave (PAW) method [14, 15]. The generalized gradient approximation (GGA) with exchange-correlation functional of Perdew, Burke and Ernzerhof (PBE) for the exchange-correlation functional [16] were employed. The kinetic energy cutoff was set to 500 eV for the plane wave basis. A $10 \times 10 \times 10$ k -mesh in self-consistent process for Brillouin zone (BZ) sampling was adopted. The experimental lattice parameters of LaNiO_2 and $\text{La}_3\text{Ni}_2\text{O}_6$ are employed [4, 11].

RESULTS AND DISCUSSIONS

Band structure and Density of states

We have first performed the first-principles calculations on LaNiO_2 without SOC. The band structure without SOC is presented in Fig. 2(a) and the total density of states (DOS) is plotted accordingly. The blue dashed horizontal line corresponds to the charge neutrality level of the un-doped compound LaNiO_2 . Based on the total number of electrons in Fig. 2(b), the red-colored dashed line is the theoretically estimated chemical potential for the 20% hole-doped superconductivity $\text{Nd}_{0.8}\text{Sr}_{0.2}\text{NiO}_2$. Moreover, the partial DOSs are also computed for O $2p$, Ni $3d$, and La $5d$ orbitals, respectively. Since the main quantum numbers of different atom's orbitals are distinct, we call them $2p$, $3d$, and $5d$ orbitals (states) for short in the following discussion. From the plotted partial DOS in Fig. 2(c), we have noticed that $2p$ states are mainly located from -10 eV to -3.5 eV below E_F , while $3d$ states are around E_F , from -3.5 eV and 1.5 eV. The situation is much different from the situation in copper-based superconductors, where O $2p$ states are slightly below E_F and hybridize strongly with Cu $3d$ states [10]. In addition, from the orbital-weighted fat bands in Fig. 2(a), we notice that there are $5d_{3z^2-r^2}$ states at Γ and $5d_{xy}$ states at A around E_F , suggesting that the $5d$ states are more extended, compared to Ca $3d$ states in CaCuO_2 [17].

Evolution of Fermi surfaces

At the charge neutrality level, we find that there are three bands crossing E_F , which are mainly from $3d_{x^2-y^2}$, $5d_{z^2}$ and $5d_{xy}$ orbitals, respectively. The weights of these orbitals are depicted by the size of different symbols in Fig. 2(a). Therefore, three EPs are formed as shown in Fig. 2(d): i) $3d_{x^2-y^2}$ orbital forms the largest electron pocket around the Γ and Z points, which has a strong 2D feature; ii) the second larger one is nearly a sphere around A , formed by $5d_{xy}$ orbital; iii) the smallest one is a sphere around Γ , formed by $5d_{3z^2-r^2}$ orbital (which is also hybridized with Ni $3d_{3z^2-r^2}$ orbital in the DFT calculations, yet we still call it $5d_{3z^2-r^2}$ for simplicity).

In the hole-doped superconductor $\text{Nd}_{0.8}\text{Sr}_{0.2}\text{NiO}_2$, the estimated chemical potential of the 20% Sr-doped level is denoted by a red-colored dashed line, which corresponds to 32.8 electrons per unit cell (The charge neutrality level corresponds to 33 electrons). Needless to say that, all the electron pockets become smaller with hole-doping. In particular, the $5d_{3z^2-r^2}$ -orbital-formed Γ -centered EP is about to be removed. On the other hand, the states from $3d_{xy}$ orbital becomes closer to the chemical potential, especially in the vicinity of A point.

TABLE I: The upper rows give the irreps for lowest six bands at in Fig. 2(a) at the maximal high-symmetry points in SG 123. The irreps are given in ascending energy order. The notation of $Zm(n)$ implies the irrep m at the Z point with the degeneracy of n . All the irrep notations are listed on the Bilbao website: www.cryst.ehu.es/cgi-bin/cryst/programs/bandrep.pl. The lower rows give the elementary band representation (EBRs), labeled as $\rho@q$. Here, ρ indicates the irrep supported by the orbital(s), while q stands for the Wyckoff site, where the orbital(s) sit. The green irreps indicate that those energy bands are at least 1.0 eV above E_F .

	A	Γ	M	Z	R	X
DFT bands	A3-(1)	GM1+(1)	M1+(1)	Z4+(1)	R4+(1)	X1+(1)
	A1+(1)	GM4+(1)	M4+(1)	Z5+(2)	R1+(1)	X4+(1)
	A5+(2)	GM5+(2)	M5+(2)		R2+(1)	X2+(1)
				Z1+(1)	R3+(1)	X3+(1)
	;	;	;	;	;	;
A4+(1)	GM2+(1)		Z2+(1)	R1+(1)	X1+(1)	
A2+(1)	GM1+(1)	M5-(2)	Z1+(1)	R2-(1)	X4-(1)	
EBRs						
$A_{1g}@1a$	A1+	GM1+	M1+	Z1+	R1+	X1+
$B_{1g}@1a$	A2+	GM2+	M2+	Z2+	R1+	X1+
$B_{2g}@1a$	A4+	GM4+	M4+	Z4+	R2+	X2+
$E_g@1a$	A5+	GM5+	M5+	Z5+	R3+	X3+
					R4+	X4+
$A_{1g}@1d$	A2-	GM1+	M4+	Z3-	R3+	X4-
$B_{2g}@1d$	A3-	GM4+	M1+	Z2-	R4+	X3-
$A_{1g}@1b$	A3-	GM1+	M1+	Z3-	R2-	X1+

Band inversion and Dirac points

The band crossings along Z-R, R-A, M-A are protected by m_{110} , m_{001} and C_{4z} , respectively. After considering SOC, the band crossings open small gaps along the mirror protected R-A and A-Z lines, but remain gapless along the C_{4z} -invariant line M-A, as shown in Fig. 2(e). The gapless Dirac points along M-A [highlighted in the red circle in Fig. 2(e)] are protected by C_{4v} symmetry. Namely, the two doubly-degenerate bands belong to different 2D irreducible representations (irreps) of C_{4v} double group. In our LDA+U calculations, we find that the band inversion is sensitive to the value of Coulomb interaction U , as we have shown in the SM.

Analysis of EBRs and Orbitals

By doing the analysis of the elementary band representations (EBR) in the theory of topological quantum chemistry [18], one can easily obtain orbital information in real space. An EBR of $\rho@q$ is labeled by the Wyckoff position q and the irrep ρ of its site symmetry group. At first, the irreps of the six low-energy bands at maximal

TABLE II: The hopping parameters for the two-band and three-band Hamiltonian.

parameters for the two-band model				parameters for the three-band model									
$t_{11}^{(0,0,0)}$	0.1470	$t_{22}^{(0,0,0)}$	0.8318	$t_{21}^{(1,0,0)}$	0.0098	$t_{11}^{(0,0,0)}$	0.0100	$t_{22}^{(0,0,0)}$	0.8280	$t_{33}^{(0,0,0)}$	-0.7960	$t_{21}^{(1,0,0)}$	0.0098
$t_{11}^{(1,0,0)}$	-0.4125	$t_{22}^{(1,0,0)}$	0.0913			$t_{11}^{(1,0,0)}$	0.0042	$t_{22}^{(1,0,0)}$	-0.0510	$t_{33}^{(1,0,0)}$	-0.1655	$t_{31}^{(1,0,0)}$	-0.0132
$t_{11}^{(0,0,1)}$	-0.0538	$t_{22}^{(0,0,1)}$	0.0650			$t_{11}^{(0,0,1)}$	0.0378	$t_{22}^{(0,0,1)}$	-0.0079	$t_{33}^{(0,0,1)}$	-0.0360	$t_{32}^{(1,1,1)}$	0.0001
$t_{11}^{(1,1,0)}$	0.0894	$t_{22}^{(1,1,0)}$	-0.0606			$t_{11}^{(1,1,0)}$	0.0043	$t_{22}^{(1,1,0)}$	0.0105	$t_{33}^{(1,1,0)}$	-0.0497		
$t_{11}^{(1,0,1)}$	0.0000	$t_{22}^{(1,0,1)}$	0.1988			$t_{11}^{(1,0,1)}$	-0.1338	$t_{22}^{(1,0,1)}$	0.0000	$t_{33}^{(1,0,1)}$	0.0105		
$t_{11}^{(1,1,1)}$	0.0134	$t_{22}^{(1,1,1)}$	0.0281			$t_{11}^{(1,1,1)}$	0.0038	$t_{22}^{(1,1,1)}$	0.0018	$t_{33}^{(1,1,1)}$	-0.0113		

high-symmetry k -points [19, 20] are computed without SOC. The results are listed in Table. I. In the crystal of LaNiO₂, the Ni atom sites at Wyckoff position 1a[0, 0, 0], while La atom sites at Wyckoff position 1d[0.5, 0.5, 0.5]. Both Wyckoff positions have the site-symmetry group of 4/*mmm*. Note that five d -orbitals only support the irreps of A_{1g} ($d_{3z^2-r^2}$), B_{1g} ($d_{x^2-y^2}$), B_{2g} (d_{xy}), and E_g ($d_{xz,yz}$) under the single group of 4/*mmm*.

The results of the EBR analysis on atomic orbitals are addressed as follows. First, by switching the irreps of A3- and A4+ at A, we can find that the four occupied bands can be represented as the sum of three EBRs: $A_{1g}@1a \oplus B_{2g}@1a \oplus E_g@1a$. Among them, the $3d_{xy}$ -based EBR $B_{2g}@1a$ has highest states at A, which may intersect with the chemical potential in the hole-doping case. Second, the band of $3d_{x^2-y^2}$ -induced EBR $B_{1g}@1a$ is clear shown by the weights in Fig. 2(a). There is no doubt that $3d_{x^2-y^2}$ orbital contributes the largest Fermi surface. Third, the irrep GM1+ at Γ is from the $5d_{3z^2-r^2}$ -induced EBR $A_{1g}@1d$. Lastly, the inverted irrep A3- is from the $5d_{xy}$ -induced ERB $B_{2g}@1d$. So far, all of the orbital compounds are consistent with our DFT calculations in Fig. 2(a).

Then, we aim to construct a minimal effective model to reproduce the bands and symmetry characteristics near E_F . Besides the $3d_{x^2-y^2}$ -induced EBR of $B_{1g}@1a$, the two irreps of A3- and GM1+ can be generated in the EBR of $A_{1g}@1b$. Therefore, we derive a two-band model, consisting of two EBRs: $B_{1g}@1a \oplus A_{1g}@1b$, which reproduce the exact irreps of symmetries near E_F from the DFT calculations. Even through there is no actually atomic orbital at Wyckoff position 1b [0,0,0.5] (with the site symmetry group 4/*mmm*), it could be formed by the hybridization of the atomic orbitals on other sites. The two-band model would be constructed for the un-doped case in the following section.

Two-band effective model

Under the basis of the B_{1g} orbital at the 1a Wyckoff position and A_{1g} orbital at the 1b Wyckoff position, the tight binding (TB) model is constructed as follows. The

diagonal terms in the Hamiltonian are

$$\begin{aligned}
T_{\alpha\alpha} = & t_{\alpha\alpha}^{(0,0,0)} + 2t_{\alpha\alpha}^{(1,0,0)}(\cos(k_x) + \cos(k_y)) \\
& + 2t_{\alpha\alpha}^{(0,0,1)}\cos(k_z) + 4t_{\alpha\alpha}^{(1,1,0)}\cos(k_x)\cos(k_y) \\
& + 4t_{\alpha\alpha}^{(1,0,1)}\cos(k_z)(\cos(k_x) + \cos(k_y)) \\
& + 8t_{\alpha\alpha}^{(1,1,1)}\cos(k_x)\cos(k_y)\cos(k_z)
\end{aligned} \quad (1)$$

where $\alpha = 1, 2$ represent the $B_{1g}@1a$ and the $A_{1g}@1b$, respectively. $t_{\beta\alpha}^{(l,m,n)}$ stands for the hopping amplitude from orbital β of the original cell to α of the (l, m, n) cell:

$$t_{\beta\alpha}^{(l,m,n)} \equiv \langle \beta; 000 | \hat{H} | \alpha; lmn \rangle \quad (2)$$

In the off-diagonal term, the nearest and next-nearest hoppings between different orbitals are given as,

$$S = t_{21}^{(1,0,0)}(1 + e^{ik_z})(4\cos(k_x) - 4\cos(k_y)) \quad (3)$$

Thus, our two-band model Hamiltonian is written as

$$H_2(k) = \begin{pmatrix} T_{11} & \dagger \\ S & T_{22} \end{pmatrix} \quad (4)$$

The fitting results are shown in the Fig. 2(f) and the parameters can be found in Table II. This two-band model can reproduce all the Fermi surfaces and symmetry characteristics obtained from the DFT calculations.

LDA+Gutzwiller method

To treat the correlation effect of five Ni 3d orbitals, we have employed the LDA+Gutzwiller method [21, 22]. The corresponding Gutzwiller trial wave function has been constructed as $|G\rangle = \hat{P}|0\rangle$ with

$$\hat{P} = \prod_i \hat{P}_i = \prod_i \sum_{\Gamma'} \lambda_{i;\Gamma'} |i, \Gamma\rangle \langle i, \Gamma'| \quad (5)$$

where $|0\rangle$ is the noninteracting wave function and \hat{P} is the Gutzwiller local projector with $|i, \Gamma\rangle$ the atomic eigenvectors on site i . $\lambda_{i;\Gamma'}$ is the so-called Gutzwiller variational parameters which adjusts the weight of different local atomic configurations. Ground states are obtained by minimizing the total energy $E = \langle G | (H_{tb} +$

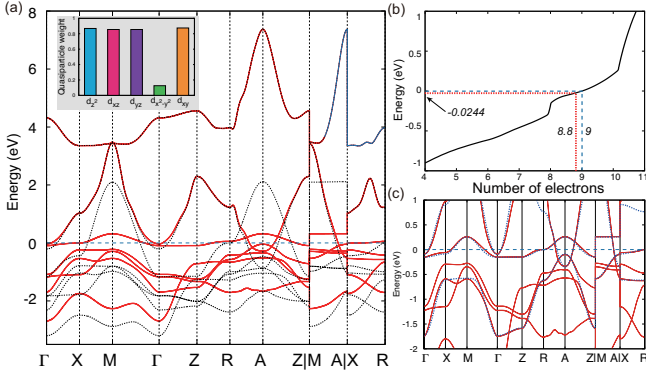


FIG. 3: (Color online) (a) The band structure of the non-interacting tight-binding Hamiltonian H_{tb} , extracted by the *Wannier90* package, is plotted in the black dashed lines, while the LDA+Gutzwiller bands are plotted in red solid lines. The inset of (a) shows the quasiparticle weights of five $3d$ orbitals. (b) shows the total number of electrons as a function of chemical potential in the LDA+Gutzwiller band structure. In panel (c), the bands of the three-band model are presented in blue dashed lines.

$H_{dc} + H_{int}|G\rangle$ with some Gutzwiller constraints. The non-interacting Hamiltonian (H_{tb}) is extracted by the *Wannier90* package [23] from the DFT calculations without SOC, which contains two La $5d_{3z^2-r^2,xy}$ orbitals and five Ni $3d$ orbitals. The double-counting term H_{dc} is given self-consistently. The on-site interacting term takes the Slater-Kanamori rotationally invariant atomic interaction [24]:

$$\begin{aligned}
 H_{int} = & U \sum_{\alpha} \hat{n}_{a\uparrow} \hat{n}_{a\downarrow} + \frac{U'}{2} \sum_{a \neq b} \sum_{\sigma \sigma'} \hat{n}_{a\sigma} \hat{n}_{b\sigma'} \\
 & - \frac{J}{2} \sum_{a \neq b} \sum_{\sigma} c_{a\sigma}^{\dagger} c_{a-\sigma} c_{b-\sigma}^{\dagger} c_{b\sigma} \\
 & - \frac{J'}{2} \sum_{a \neq b} c_{a\uparrow}^{\dagger} c_{a\downarrow}^{\dagger} c_{b\uparrow} c_{b\downarrow}
 \end{aligned} \quad (6)$$

where $c_{a\sigma}^{\dagger}$ ($c_{a\sigma}$) creates (annihilates) an electron in the state of the orbital a and the spin σ , and $\hat{n}_{a\sigma} = c_{a\sigma}^{\dagger} c_{a\sigma}$.

For simplicity, we adopt diagonal variational parameters which means $\lambda_{i;\Gamma\Gamma'} = \lambda_{i;\Gamma}\delta_{\Gamma\Gamma'}$ here. Five Ni $3d$ orbitals are treated as correlated orbitals in the calculation (which correspond to 10 bands once considering the spin degree of freedom). We take Coulomb interaction U of 5 eV, Hund's coupling J of $0.18U$, $U' = U - 2J$ and $J' = J$. Besides, the occupancy of Ni $3d$ orbitals has been forced to be 8.462 obtained from the DFT calculations. The results show that the quasi-particle weight of $d_{x^2-y^2}$ orbital is very small, 0.12, while the weights of other four orbitals are about 0.85. After considering the renormalization of the correlated $3d$ orbitals, the modified band structure is obtained, as shown in Fig. 3(a). Two significant features are found after our Gutzwiller correction: one is that the bandwidth of $3d_{x^2-y^2}$ has been renormal-

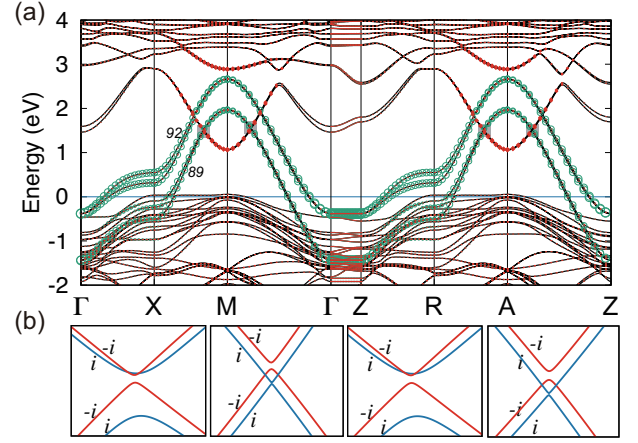


FIG. 4: (Color online) (a) The ferromagnetic band structure of $\text{La}_3\text{Ni}_2\text{O}_6$ with SOC. The weights of La $5d_{xy}$ and Ni $3d_{x^2-y^2}$ states are indicated by the size of red diamonds and green circles, respectively. (b) The crossing points between 90 and 91 bands. Bands with different mirror eigenvalues are printed as blue (for $+i$) and red (for $-i$) lines.

ized largely, leading to a DOS peak around Fermi level, which may contribute to the large peak around zero energy in RIXS spectrum[25]; the other is that the $3d_{xy}$ states near A point become very close to E_F . As a result, a HP could be induced by hole doping, which may be related to the observed sign change of Hall coefficient.

In addition, the band inversion between the $3d_{xy}$ states and $5d_{xy}$ states near A point could be important in the hole-doped nickelate compound $\text{Nd}_{0.8}\text{Sr}_{0.2}\text{NiO}_2$, since they are very close to E_F . Therefore, we modify our model by simply adding an additional $3d_{xy}$ orbital to capture the potential band inversion in this hole-doped compound. The modified model is written as,

$$H_3(k) = \begin{pmatrix} T_{11} & \dagger \\ S & T_{22} \\ W & P & T_{33} \end{pmatrix} \quad (7)$$

$$\text{with } P = 4t_{31}^{(1,0,0)}(1 + e^{1k_z})(\cos(k_x) - \cos(k_y))$$

$$W = 8t_{32}^{(1,1,1)} \cos(k_x) \cos(k_y) \cos(k_z)$$

The parameters are obtained by fitting with the renormalized bands, as shown in Table II. The results of the modified model $H_3(k)$ are shown in Fig. 3(c), which fit very well with the LDA+Gutzwiller bands, which can be compared with the ARPES experimental data. In any case, a four-band model constructed totally from the real atomic orbitals are presented in the SM.

Ferromagnetic state in $\text{La}_3\text{Ni}_2\text{O}_6$

Band topology can also be found in another member of the T' type $\text{Ln}_{n+1}\text{Ni}_n\text{O}_{2n+2}$ homologous series, for

example the ferromagnetic state of $\text{La}_3\text{Ni}_2\text{O}_6$ ($n = 2$), whose band structure with SOC is shown in Fig. 4(a). The z -oriented magnetism reduces the symmetry from type-II magnetic SG 139 to type-I magnetic SG 87. Near the M/A point, the four downward parabolic bands (*i.e.*, 89-92 bands) are mainly from the $3d_{x^2-y^2}$ states of Ni atoms in two planar Ni-O layers, while the two upward parabolic bands (*i.e.*, 93-94 bands) are mainly from the $5d_{xy}$ states of the La atoms sandwiching by the two Ni-O planes [Fig. 1(b)]. Once looking closely at the crossings between 90th and 91st bands in Fig. 4(b), we found that there is a gap along X-M (R-A), while there are two crossing points along M- Γ (A-Z). These crossing points are parts of the tiny M_z -protected nodal rings at $k_z = 0, 2\pi/c$ planes, which can be easily removed by very small perturbations (without changing the ordering of energy bands at high-symmetry k -points). According to symmetry indicators defined in magnetic systems[26], insulators in type-I MSG 87 is characterized by the indicators $\mathbb{Z}_4 \times \mathbb{Z}_4$ [27, 28], which can be explained by two mirror Chern numbers in the $k_z = 0$ plane. By using the C_4 eigenvalues[29], we find that the Chern numbers are 0, 2 for the mirror eigenvalue $\pm i$ sectors, respectively, which indicate that non-trivial edge states can emerge on the M_z -preserving surface.

CONCLUSION

Based on our first-principles calculations, we find that, in the un-doped case, there are three EPs: a largest EP from Ni $3d_{x^2-y^2}$ orbital, a small one at Γ from La $5d_{3z^2-r^2}$ orbital and a relatively bigger one at A from La $5d_{xy}$. These Fermi surfaces and symmetry characteristics can be reproduced by our two-band model, which consists of two elementary band representations: $B_{1g}@1a \oplus A_{1g}@1b$. In the obtained band structure, there is a band inversion happened near A, which gives rise to a pair of Dirac points along A-M once including SOC. The correlation effect of Ni $3d$ orbitals have been estimated in our LDA+Gutzwiller calculation, and the renormalized band structure is obtained, which indicates that Ni $3d_{xy}$ states become very close to E_F near A point. A hole pocket is likely induced by hole doping, which may be related to the observed sign change of Hall coefficient. The hole-pocket band and the band inversion can be captured in the modified model by simply including another Ni $3d_{xy}$ orbital. In addition, we show that the nontrivial band topology in the ferromagnetic two-layer compound $\text{La}_3\text{Ni}_2\text{O}_6$ is associated with Ni $3d_{x^2-y^2}$ and La $5d_{xy}$ orbitals.

Note added. At the stage of finalising the present paper, we are aware of the similar works on nickelates[30–34].

Acknowledgments We thank Jinguang Cheng for

drawing our attention to this subject and valuable discussion, as well as critical reading of this work. This work was supported by the National Natural Science Foundation of China (11974395, 11504117, 11774399, 11622435, U1832202), Beijing Natural Science Foundation (Z180008), the Ministry of Science and Technology of China (2016YFA0300600, 2016YFA0401000 and 2018YFA0305700), the Chinese Academy of Sciences (XDB28000000, XDB07000000), the Beijing Municipal Science and Technology Commission (Z181100004218001, Z171100002017018). H.W. acknowledges support from the Science Challenge Project (No. TZ2016004), the K. C. Wong Education Foundation (GJTD-2018-01). Z.W. acknowledges support from the CAS Pioneer Hundred Talents Program and the National Thousand-Young-Talents Program.

* Electronic address: wzj@iphy.ac.cn

† Electronic address: cfang@iphy.ac.cn

‡ Electronic address: hmweng@iphy.ac.cn

- [1] J. G. Bednorz and K. A. Müller, *Zeitschrift für Physik B Condensed Matter* **64**, 189 (1986).
- [2] M.-K. Wu, J. R. Ashburn, C. Torng, P. H. Hor, R. L. Meng, L. Gao, Z. J. Huang, Y. Wang, and a. Chu, *Physical review letters* **58**, 908 (1987).
- [3] V. Anisimov, D. Bukhalov, and T. Rice, *Physical Review B* **59**, 7901 (1999).
- [4] D. Li, K. Lee, B. Y. Wang, M. Osada, S. Crossley, H. R. Lee, Y. Cui, Y. Hikita, and H. Y. Hwang, *Nature* **572**, 624 (2019).
- [5] M. Hayward, M. Green, M. Rosseinsky, and J. Sloan, *Journal of the American Chemical Society* **121**, 8843 (1999).
- [6] M. Hayward and M. Rosseinsky, *Solid state sciences* **5**, 839 (2003).
- [7] E. Motoyama, G. Yu, I. Vishik, O. Vajk, P. Mang, and M. Greven, *Nature* **445**, 186 (2007).
- [8] P. A. Lee, N. Nagaosa, and X.-G. Wen, *Reviews of modern physics* **78**, 17 (2006).
- [9] M. Smith, A. Manthiram, J. Zhou, J. B. Goodenough, and J. T. Markert, *Nature* **351**, 549 (1991).
- [10] K.-W. Lee and W. Pickett, *Physical Review B* **70**, 165109 (2004).
- [11] V. V. Poltavets, M. Greenblatt, G. H. Fecher, and C. Felser, *Phys. Rev. Lett.* **102**, 046405 (2009), URL <https://link.aps.org/doi/10.1103/PhysRevLett.102.046405>.
- [12] G. Kresse and J. Furthmüller, *Computational Materials Science* **6**, 15 (1996), ISSN 0927-0256, URL <http://www.sciencedirect.com/science/article/pii/0927025696000080>.
- [13] G. Kresse and J. Furthmüller, *Phys. Rev. B* **54**, 11169 (1996), URL <https://link.aps.org/doi/10.1103/PhysRevB.54.11169>.
- [14] P. E. Blöchl, *Phys. Rev. B* **50**, 17953 (1994), URL <https://link.aps.org/doi/10.1103/PhysRevB.50.17953>.
- [15] G. Kresse and D. Joubert, *Phys. Rev. B* **59**, 1758 (1999), URL <https://link.aps.org/doi/10.1103/PhysRevB.59.1758>.

- 59.1758.
- [16] J. P. Perdew, K. Burke, and M. Ernzerhof, Phys. Rev. Lett. **77**, 3865 (1996), URL <https://link.aps.org/doi/10.1103/PhysRevLett.77.3865>.
 - [17] H. Wu, Q.-q. Zheng, X.-g. Gong, and H. Lin, Journal of Physics: Condensed Matter **11**, 4637 (1999).
 - [18] B. Bradlyn, L. Elcoro, J. Cano, M. Vergniory, Z. Wang, C. Felser, M. Aroyo, and B. A. Bernevig, Nature **547**, 298 (2017).
 - [19] J. Gao, Q. Wu, C. Persson, and Z. Wang, arXiv preprint arXiv:2002.04032 (2019), URL <https://arxiv.org/abs/2002.04032>.
 - [20] M. Vergniory, L. Elcoro, C. Felser, N. Regnault, B. A. Bernevig, and Z. Wang, Nature **566**, 480 (2019).
 - [21] X. Deng, L. Wang, X. Dai, and Z. Fang, Phys. Rev. B **79**, 075114 (2009), URL <https://link.aps.org/doi/10.1103/PhysRevB.79.075114>.
 - [22] L. Du, L. Huang, and X. Dai, The European Physical Journal B **86**, 94 (2013), URL <https://link.springer.com/article/10.1140%2Fepjb%2Fe2013-31024-6>.
 - [23] N. Marzari, A. A. Mostofi, J. R. Yates, I. Souza, and D. Vanderbilt, Rev. Mod. Phys. **84**, 1419 (2012), URL <https://link.aps.org/doi/10.1103/RevModPhys.84.1419>.
 - [24] N. Lanatà, H. U. R. Strand, X. Dai, and B. Hellsing, Phys. Rev. B **85**, 035133 (2012), URL <https://link.aps.org/doi/10.1103/PhysRevB.85.035133>.
 - [25] M. Hepting, D. Li, C. J. Jia, H. Lu, E. Paris, Y. Tseng, X. Feng, M. Osada, E. Been, Y. Hikita, et al., Nature Materials (2020).
 - [26] A. M. Turner, Y. Zhang, R. S. K. Mong, and A. Vishwanath, Phys. Rev. B **85**, 165120 (2012), URL <https://link.aps.org/doi/10.1103/PhysRevB.85.165120>.
 - [27] H. C. Po, A. Vishwanath, and H. Watanabe, Nature communications **8**, 50 (2017).
 - [28] S. Ono and H. Watanabe, Physical Review B **98**, 115150 (2018).
 - [29] C. Fang, M. J. Gilbert, and B. A. Bernevig, Physical Review B **86**, 115112 (2012).
 - [30] J. Hirsch and F. Marsiglio, arXiv preprint arXiv:1909.00509 (2019).
 - [31] H. Sakakibara, H. Usui, K. Suzuki, T. Kotani, H. Aoki, and K. Kuroki, arXiv preprint arXiv:1909.00060 (2019).
 - [32] A. S. Botana and M. R. Norman, arXiv preprint arXiv:1908.10946 (2019).
 - [33] W. Xianxin, S. Domenico, Di, S. Tilman, H. Werner, Y. Harold, R. Srinivas, and T. Ronny, arXiv preprint arXiv:1909.03015 (2019).
 - [34] Y. Nomura, H. Motoaki, T. Terumasa, Y. Yoshhide, N. Kazuma, and A. Ryotaro, arXiv preprint arXiv:1909.03942 (2019).

SUPPLEMENTARY MATERIAL

A. The band structures of different compounds $LnNiO_2$ ($Ln=La, Pr, Nd$)

The band structures are in our DFT calculations with SOC for the $LnNiO_2$ ($Ln=La, Pr, Nd$) compounds.

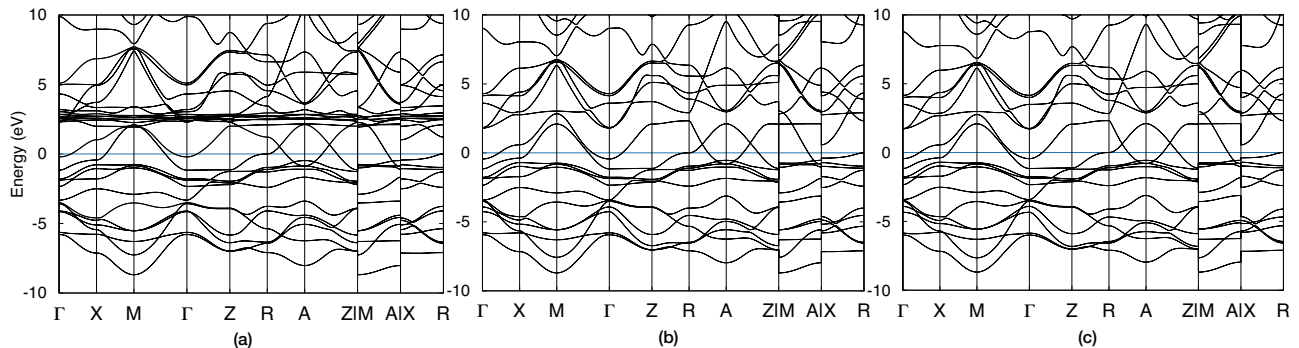


FIG. S1: (Color online) Band structures of $LaNiO_2$ (a), $PrNiO_2$ (b) and $NdNiO_2$ (c). The $4f$ states of Pr and Nd treated as core states in our PAW potential in our VASP calculations.

B. The evolution of band structures with different U values

The band structure can be affected by the Coulomb interaction, which can be simulated by using the LDA+ U method as implemented in VASP. Here we add the on-site interaction on Ni- $3d$ orbitals from $U = 1\text{eV}$ to $U = 6\text{eV}$ in the $LaNiO_2$ compound. The interaction does not change the overall band structure very much. But, the relative energy difference between the bands of four $3d$ orbitals (except $d_{x^2-y^2}$) and the other bands (*i.e.*, $3d_{x^2-y^2}$, $5d_{xy}$) increases monotonically as increasing U . As shown in Fig. S2, the band inversion can be removed when $U = 6\text{eV}$, resulting the disappearance of Dirac points.

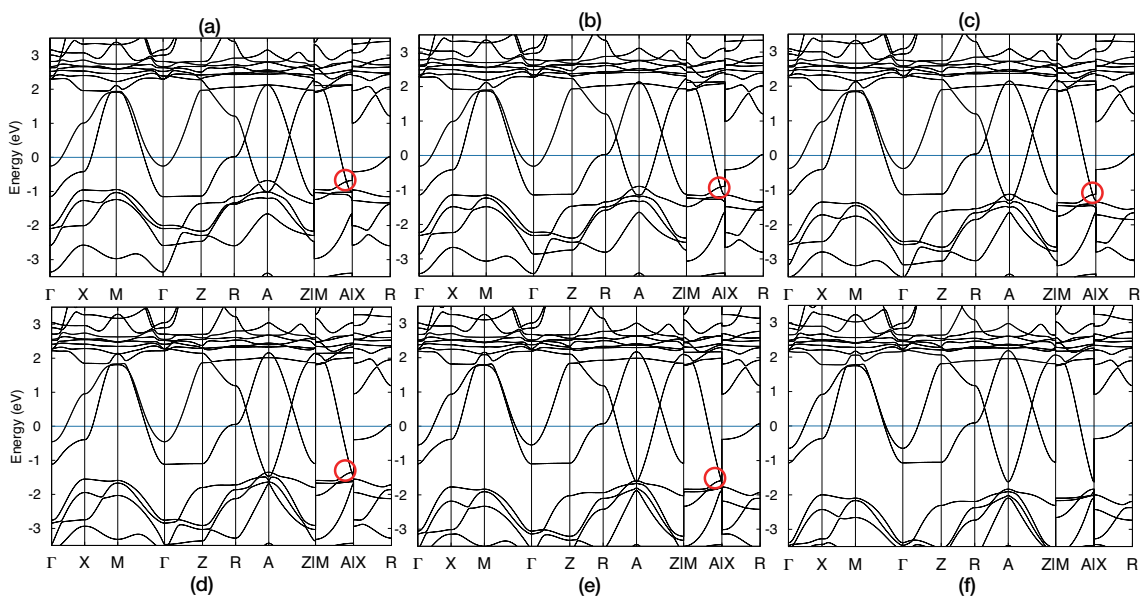


FIG. S2: (Color online) Band structure of $LaNiO_2$ under different Coulomb interactions, from $U = 1\text{eV}$ (a) to $U = 6\text{eV}$ (f). The Dirac point concerned are indicated by red circles.

C. Irreducible representations for DFT bands with SOC

The irreps of the energy bands with SOC at maximal high-symmetry points are give in Table S1. By using the opensource codes of topological quantum chemistry [18–20], the results indicate that it's a Dirac semimetal with 8 occupied bands.

TABLE S1: The irreducible representations (irreps) for the eight occupied bands (4 doubly-degenerate ones) with SOC at the maximal high-symmetry points in SG 123. The irreps are given in ascending energy order. The notation of $Zm(n)$ implies the irrep m at the Z point with the degeneracy of n .

A	Γ	M	R	X	Z
A9(2)	GM7(2)	M7(2)	Z6(2)	R5(2)	X5(2)
A7(2)	GM6(2)	M6(2)	Z7(2)	R5(2)	X5(2)
A7(2)	GM7(2)	M7(2)	Z6(2)	R5(2)	X5(2)
A6(2)	GM6(2)	M6(2)	Z7(2)	R5(2)	X5(2)

D. The four-band model

Here we construct a four band TB model to capture the band topology and Fermi surface structure by using the real atoms' orbitals, in case anyone needs the real atomic orbitals to determine the interacting strength. Based on the analysis of orbital components, we choose our orbitals as: La- d_{xy} , La- d_{z^2} , Ni- $d_{x^2-y^2}$, Ni- d_{xy} , which are referred to as $\alpha = 1, 2, 3, 4$, respectively. The four-band model reads as:

$$H_4(k) = \begin{pmatrix} H_{11} & & & \dagger \\ H_{21} & H_{22} & & \\ H_{31} & H_{32} & H_{33} & \\ H_{41} & H_{42} & H_{43} & H_{44} \end{pmatrix} \quad (8)$$

The space group \mathcal{G} is $P4/mmm$, generated by discrete translation symmetry, inversion, C_{4z} , C_{2x} and C_{2y} .

$$t_{\beta\alpha}^{(l,m,n)} \equiv \langle \beta; 000 | \hat{H} | \alpha; lmn \rangle \quad (9)$$

The diagonal terms have the same form as Eq (1) in the main text

$$\begin{aligned} H_{\alpha\alpha} = & t_{\alpha\alpha}^{(0,0,0)} + 2t_{\alpha\alpha}^{(1,0,0)}(\cos(k_x) + \cos(k_y)) \\ & + 2t_{\alpha\alpha}^{(0,0,1)}\cos(k_z) + 4t_{\alpha\alpha}^{(1,1,0)}\cos(k_x)\cos(k_y) \\ & + 4t_{\alpha\alpha}^{(1,0,1)}\cos(k_z)(\cos(k_x) + \cos(k_y)) \\ & + 8t_{\alpha\alpha}^{(1,1,1)}\cos(k_x)\cos(k_y)\cos(k_z) \end{aligned} \quad (10)$$

where $t_{\beta\alpha}^{(l,m,n)}$ stands for the hopping amplitude from orbital β of the original cell to α of the (l, m, n) cell as shown in Fig. S3(a):

The anti-diagonal terms are listed as follows

$$H_{21} = 2t_{21}^{(1,1,0)}(\cos(k_x + k_y) - \cos(k_x - k_y)) \quad (11)$$

$$H_{31} = t_{31}^{(1,0,0)}(1 + e^{ik_z})[(1 - e^{ik_y})(e^{-ik_x} - e^{2ik_x}) + (1 - e^{ik_x})(e^{2ik_y} - e^{-ik_y})] \quad (12)$$

$$H_{32} = t_{32}^{(1,0,0)}(1 + e^{ik_z})[(1 + e^{ik_y})(e^{2ik_x} + e^{-ik_x}) - (1 + e^{ik_x})(e^{2ik_y} + e^{-ik_y})] \quad (13)$$

$$H_{41} = t_{41}^{(0,0,0)}(1 + e^{ik_z})(1 + e^{ik_x})(1 + e^{ik_y}) \quad (14)$$

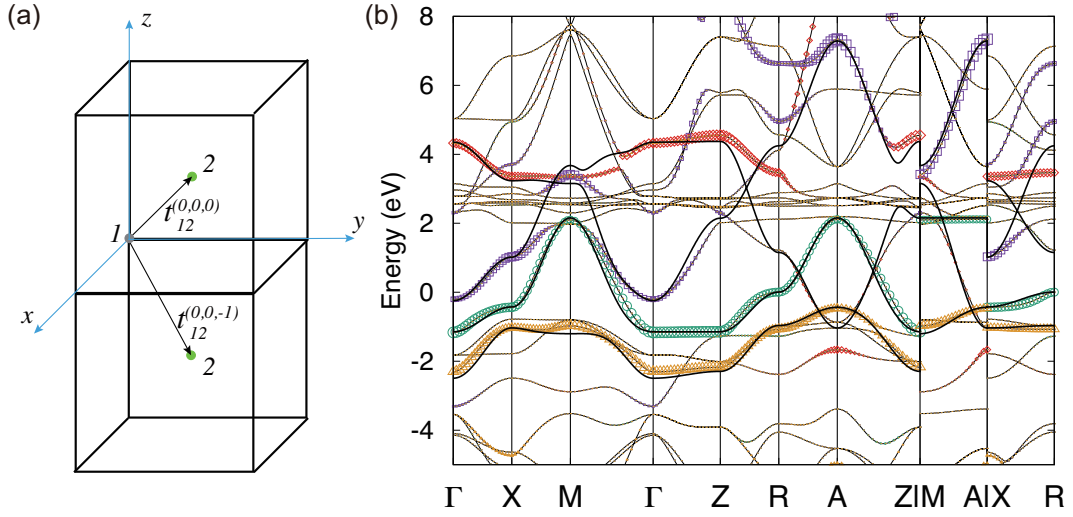


FIG. S3: (Color online) (a) Hopping between different orbitals (b) Band structure of four band tight binding model (black solid line).

TABLE S2: The hopping parameters for the four-band Hamiltonian

$t_{11}^{(0,0,0)}$	2.4319	$t_{22}^{(0,0,0)}$	2.8954	$t_{33}^{(0,0,0)}$	0.1470	$t_{44}^{(0,0,0)}$	-1.2546	$t_{21}^{(1,1,0)}$	0.2720
$t_{11}^{(1,0,0)}$	0.4031	$t_{22}^{(1,0,0)}$	-0.5519	$t_{33}^{(1,0,0)}$	-0.4125	$t_{44}^{(1,0,0)}$	-0.2013	$t_{31}^{(1,0,0)}$	-0.0281
$t_{11}^{(0,0,1)}$	0.5106	$t_{22}^{(0,0,1)}$	-0.7931	$t_{33}^{(0,0,1)}$	-0.0536	$t_{44}^{(0,0,1)}$	-0.0450	$t_{32}^{(1,0,0)}$	0.0281
$t_{11}^{(1,1,0)}$	0.0597	$t_{22}^{(1,1,0)}$	0.0659	$t_{33}^{(1,1,0)}$	0.0894	$t_{44}^{(1,1,0)}$	-0.0638	$t_{41}^{(0,0,0)}$	-0.1286
$t_{11}^{(1,0,1)}$	-0.1366	$t_{22}^{(1,0,1)}$	0.0453	$t_{33}^{(1,0,1)}$	0.0000	$t_{44}^{(1,0,1)}$	0.0156	$t_{42}^{(0,0,0)}$	0.1366
$t_{11}^{(1,1,1)}$	-0.0023	$t_{22}^{(1,1,1)}$	0.0036	$t_{33}^{(1,1,1)}$	0.0134	$t_{44}^{(1,1,1)}$	-0.0069	$t_{43}^{(1,1,1)}$	0.0001

$$H_{42} = t_{42}^{(0,0,0)}(1 + e^{ik_z})(1 - e^{ik_x})(1 - e^{ik_y}) \quad (15)$$

$$H_{43} = 8t_{43}^{(1,1,1)} \cos(k_x) \cos(k_y) \cos(k_z) \quad (16)$$

Using the parameters listed in Table. S2, the band structure of the four band model are shown in Fig. S3(b).